Post-fire residual strength and DSM-based predictions of cold-formed steel columns undergoing distortional collapse

http://dx.doi.org/10.1590/0370-44672025790007

Gabriela Ribeiro Fernandes[1,3]
https://orcid.org/0000-0002-8958-1555
Fernanda Cristina Moreira Da Silva Costa[2,4]
https://orcid.org/0000-0002-2035-9892
Alexandre Landesmann[1,5]
https://orcid.org/0000-0002-3974-5953

[1]Universidade Federal do Rio de Janeiro - UFRJ,
COPPE – Instituto Alberto Luiz Coimbra,
Programa de Engenharia Civil,
Rio de Janeiro – Rio de Janeiro - Brasil.

[2]Universidade Federal Rural do Rio de Janeiro - UFRRJ,
Instituto de Tecnologia,
Departamento de Arquitetura e Urbanismo,
Rio de Janeiro – Rio de Janeiro - Brasil.

E-mails: [3]gabriela.fernandes@coc.ufrj.br,
[4]fernandacosta@ufrrj.br, [5]alandes@coc.ufrj.br

Abstract

This article aims to investigate the residual structural behavior, strength and Direct Strength Method (DSM) design of cold-formed steel (CFS) columns that fail in distortional modes after exposure to elevated temperatures from fire (post-fire conditions). It specifically examines the influence of temperature-dependent material properties of cold-formed steel on the residual strength of fixed-end lipped-channel (LC) columns after exposure to seven temperatures (*T=20–300–400–500–600–700–800* ºC) and subsequent cooling, as reported in literature. Residual failure load data for the columns, obtained through ANSYS shell finite element analysis (SFEA), are employed to evaluate the impact of temperature-dependent steel constitutive models on the predictive accuracy of existing DSM distortional strength curves. The findings demonstrate that the current DSM distortional design curve for room temperature effectively addresses distortional failures in post-fire scenarios.

Keywords: cold-formed steel columns; distortional post-buckling behavior; post-fire residual strength; ANSYS shell finite element investigation; Direct Strength Method (DSM) design.

1. Introduction

The utilization of cold-formed steel (CFS) members has experienced substantial growth in recent years, driven by the construction sector's demand for cost-efficient production methods and fabrication flexibility. Among these, CFS frame walls have gained prominence in both residential and industrial applications, offering an adaptable and economical design solution. However, similar to all structural systems, these members are susceptible to accidental fire incidents. Furthermore, CFS members are inherently prone to various instability phenomena, which frequently govern their structural capacity and safety. Under fire conditions, these instability issues become even more pronounced, underscoring the limited body of research on the residual strength of such elements after being exposed to elevated temperatures. This knowledge gap poses significant challenges in reliably assessing the potential for reuse of these structural systems following exposure to elevated temperatures.

Outinen and Mäkeläinen (2004) were among the first to investigate the mechanical properties of structural steel at elevated temperatures and subsequent cooling. While no specific expressions for calculating these properties were proposed, their research marked a foundational contribution to the study of post-fire behavior. In recent years, a significant increase in research addressing the performance of cold-formed steel members following fire exposure has been observed. The normative expressions based on the Direct Strength Method (DSM) (e.g., Schafer, 2008), found in the current versions of the North American (AISI, 2020), Australian/New Zealand (AS/NZS, 2018), and Brazilian (ABNT, 2010) specifications for CFS structures, lack guidance on evaluating the residual strength or designing for the reuse of structures exposed to fire. British Standard 5950, Part 8, Appendix B (BS, 1990), provides limited guidance on the reuse of structural steel after fire, stating that reuse is allowed if distortions remain within tolerances for straightness and shape. Additionally, Appendix J of the Chinese Standard CECS 252:2009 (CECS, 2009) provides yield strength reduction factors for hot-rolled structural steels under fire conditions and after cooling. These reduction factors, however, may not be applicable to other types of steel, such as CFS.

In recent years, several researchers (*e.g.*, Gunalan and Mahendran, 2014 a,b; Lu *et al.*, 2016; Kesawan and Mahendran, 2017; Li and Young, 2018; Singh and Singh, 2018; Yu *et al.*, 2019; Cai and Young, 2019; Chen *et al.*, 2019; Ren *et al.*, 2020; Pandey and Young, 2021; Shi *et al.*, 2022) have conducted experimental studies on CFS samples to evaluate their behavior and residual capacities after exposure to elevated temperatures. Based on the results, these authors have proposed expressions for the reduction factors of mechanical properties. Figure 1 illustrates the variation of these reduction factors with temperature. It is noteworthy that there is considerable dispersion in the values, which reflects the variability in post-fire behaviors observed across different studies. Despite these efforts, the only (post-fire) numerical study available in literature is that of Gunalan and Mahendran (2014 a,b). In fact, investigating the residual strength of cold-formed steel members that fail by distortional buckling is crucial for evaluating their post-fire structural performance, given the sensitivity of this failure mode to high temperatures. As current design standards lack specific guidance for post-fire scenarios, such studies support the development of more accurate design methods, enable safe reuse of structural elements, and enhance sustainability and safety in fire-affected buildings. Therefore, the objective of the present research is to expand upon the study of Gunalan and Mahendran (2014 a,b) by: (i) utilizing the validated model to perform a series of SFE analyses conducted using ANSYS to investigate the distortional buckling behavior of CFS compression members subjected to post-fire conditions; and (ii) finally, evaluating whether the current DSM design equation can accurately and safely predict the residual strength of CFS columns under distortional buckling or failure modes. This article specifically focuses on lipped channel (LC) columns with fixed-end support conditions subjected to seven temperatures (*T*=20–300–400–500–600–700–800 °C). Indeed, the reduction factors reported by eleven previous studies (see Figure 1) are integrated into the numerical model to analyze the distortional buckling behavior of CFS columns post-fire, contributing to a long-term assessment and potential benefits for reuse of CFS under varying fire scenarios and load conditions.

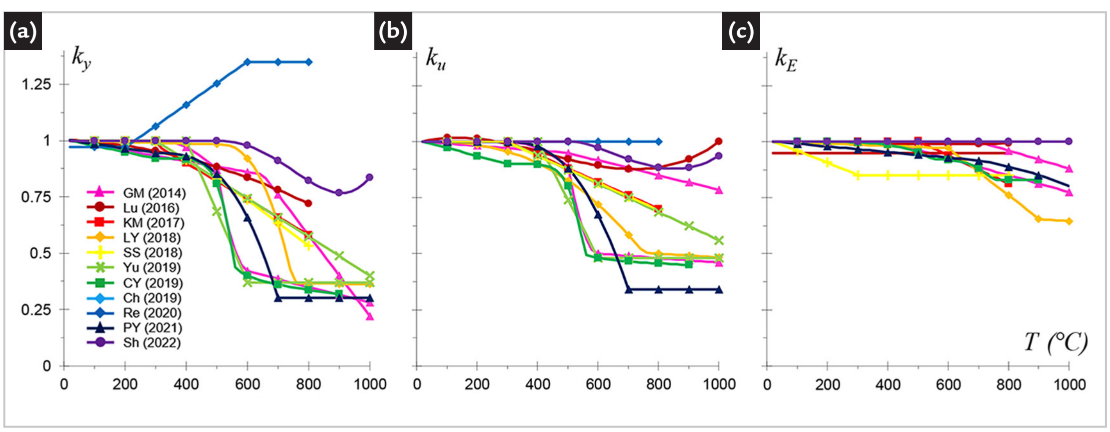

Figure 1 - Reduction factors proposed by researchers for post-fire CFS structures (concerning flat specimens) after air-cooling: (a) k_y, (b) k_u, and (c) k_E. The legend acronyms correspond to the following authors: Gunalan and Mahendran – GM; Lu *et al.* – Lu; Kesawan and Mahendran – KM; Li and Young – LY; Singh and Singh – SS; Yu *et al.* – Yu; Cai and Young – CY; Chen *et al.* – Ch; Ren *et al.* – Re; Pandey and Young – PY; Shi *et al.* – Sh.

2. Selection of column geometry and buckling response

The initial step of this study focused on selecting the appropriate cross-sectional dimensions and length for the lipped channel cold-formed steel columns to be analyzed, assuming a fixed-end condition that restrains global (major and minor-axis) and local rotations, warping and torsional displacements. The column geometry selection process involved performing buckling analyses using two methods: (i) the GBTul code, derived from Generalized Beam Theory (GBT) by Bebiano *et al.* (2008 a,b), and (ii) ANSYS shell finite element analysis (SAS, 2009). As a result, the C200 cross-section was proposed (see dimensions in Figure 2a) and a distortional buckling length (L_D) of 110 cm. The curves in Figure 2(b) illustrate the variation of elastic critical buckling loads, $P_{cr.T}$, with column length L (logarithmic scale) for the selected C200x200 column. These curves are derived from seven temperature levels (*T=20–300–400–500–600–700–800* °C), employing the constitutive model proposed by Gunalan and Mahendran (2014 a,b), as detailed in Section 3.1. The critical (distortional) buckling modes of the column are depicted in Figure 2(c). Each buckling curve represents a 'vertical shift' of the reference curve, with the extent of the displacement solely dependent on the reduction in Young's modulus due to the increase in temperature.

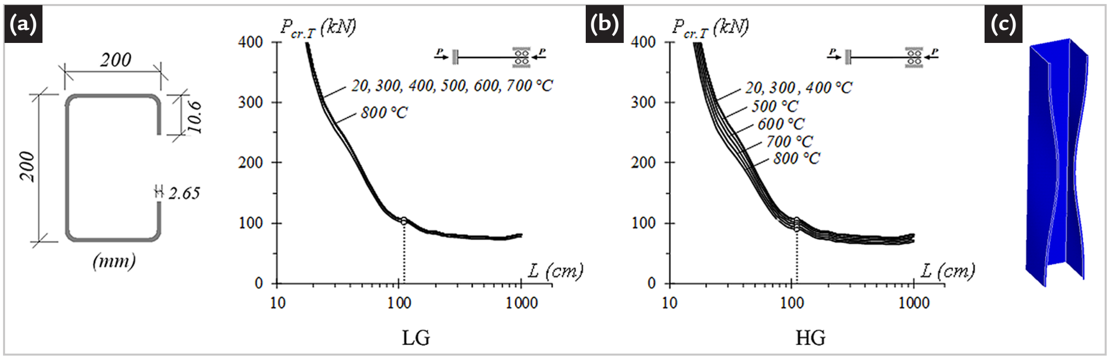

Figure 2 - (a) C200 cross-section dimensions, (b) variation of $P_{cr.T}$ with L and T low grade (LG) and high grade (HG) steels (Gunalan and Mahendran, 2014 a,b); (c) distortional critical buckling mode shape.

3. FE-modelling of CFS columns

The post-buckling behavior of the columns under distortion was analyzed using ANSYS software (SAS, 2009). A previously validated shell finite element model developed by Landesmann and Camotim (2011) was used to discretize the columns into high-resolution meshes made up of Shell181 elements. These elements are 4-node thin-shell elements that include shear deformation capabilities, providing six degrees of freedom per node and utilizing full integration. Convergence studies indicated that a mesh size of 5 mm by 5 mm produced accurate results while maintaining computational efficiency. The analyses were carried out employing an incremental-iterative method that integrates the Newton-Raphson approach with an arc-length control strategy. This methodology accurately models the behavior of columns subjected to a uniform temperature distribution (steady test), simulating conditions where the columns are exposed to both flames and ambient air temperature (Landesmann and Camotim, 2011). Indeed, while the steady state is more easily controlled in experimental tests, directly providing the stress-strain curve, the transient state is more representative of a real fire situation, because the temperatures increase over time and the load is usually stable. Moreover, in the transient state, the results lead to temperature curves varying in function of deformation and it is necessary to convert these results to obtain the usual stress-strain curve – more complex and imprecise methodology. Therefore, only steady-state tests are considered herein. Following the temperature application, the columns were subjected to axial compression until failure occurred. The outcomes of these steady-state analyses provided critical insights into the failure loads. For modelling the fixed (F) end support conditions, the following assumptions were made: (i) at the fixed support, the column's end section was rigidly connected to a plate, preventing any local or global displacements, rotations, and warping; (ii) to allow the application of axial loads, axial translation was left unconstrained at both end sections. Axial compression was applied through concentrated forces at the centroid of the end section, corresponding to the rigid plate. These forces were incrementally increased in small steps, using the automatic load-stepping feature available in ANSYS (SAS, 2009). This methodology ensured the precise and reliable simulation of post-buckling behavior under the applied loading conditions. Each of the columns analyzed included initial geometric imperfections with a critical (distortional) shape and small amplitude (10% of the wall thickness, t). These imperfections, characterized by inward flange-stiffener motions, were based on the distortional post-buckling asymmetry studies by Prola and Camotim (2002 a,b) and Silvestre and Camotim (2006), which have demonstrated that such imperfections result in reduced post-buckling strength. The critical buckling mode shape for each column was determined through an initial ANSYS buckling analysis, using the same shell finite element mesh employed in the subsequent nonlinear (post-buckling) analysis. This approach enables easy conversion of the buckling analysis output into input for the nonlinear analysis. Additionally, it is important to note that residual stresses and corner strength effects were excluded from this study, as previous research (*e.g.*, Ellobody and Young, 2005) suggests their combined effect on column strength is negligible.

To evaluate the consistency of the distortional buckling behavior and ultimate load capacities of the model developed in this research, these values were compared with the study by Gunalan and Mahendran (2014 a,b). In this study, the researchers proposed a series of *27* compression tests of fire-exposed, short-lipped channel columns made of varying steel grades (*G300, G500* and *G550*) and thicknesses (*0.95, 1.00* and *1.15* mm). The ultimate failure loads were recorded during the tests and used for comparison with the values obtained from appropriate finite element models via ABAQUS Standard Version 6.7 (ABAQUS, 2007). These numerical results of residual strength were compared with the results obtained from the model developed in this research using ANSYS software (SAS, 2009). The examination of these results yields the following observations: (i) *13* columns exhibited inward buckling, while *12* showed outward buckling; (ii) the average ultimate load values from this study, compared with those from Gunalan and Mahendran (2014 a,b), were *1.006* (inward) and *0.963* (outward), with standard deviations of *0.070* (inward) and *0.067* (outward) and a coefficient of variation of *0.069* for both cases (inward/outward); (iii) overall, the numerical model effectively captured distortional buckling behavior and ultimate load capacity in cold-formed steel columns. This model can also be applied, with necessary adjustments to mechanical properties of material, to investigate steel columns with different yield strengths.

3.1 Fire-affected steel constitutive law

The distortional post-buckling residual behavior of the CFS C200 column is simulated in the ANSYS software (SAS, 2009) using a series of plastic strain/yield stress points to represent the fire-affected steel constitutive law. The constitutive law for the post-fire residual strength of steel adopted in this study is based on analytical expressions proposed by Gunalan and Mahendran (2014 a,b), which extend earlier works by Mander (1983), Boeraeve (1993), and Wang (2012). Gunalan and Mahendran (2014 a,b) suggest that, under post-fire conditions, the residual stress-strain curves for high-strength steels can be approximated as elastic-perfectly plastic when the maximum exposure temperature does not exceed *500 °C*. For high-grade steels exposed to temperatures above *550* °C and low-grade steels exposed to temperatures up to *800 °C*, the stress-strain response features a clear yield plateau followed by strain hardening. As a result, the residual stress-strain behavior is characterized by four distinct regions, as shown in Figure 3 and defined by Eq. (1) (Mander, 1983; Boeraeve, 1993; Wang, 2012).

The stress-strain curve begins with (i) a linear-elastic region with a slope equal to E_T (E_{20} = 205 GPa), up to the residual yield stress (σ_{yT}). This is followed by (ii) a yield plateau, during which the material deforms plastically until the onset of strain hardening (ε_{pT}). Subsequently, (iii) a strain-hardening phase occurs, where the material reaches its ultimate strength (σ_{uT}) and ultimate strain (ε_{uT}). Finally, (iv) the curve concludes with necking and material failure. Throughout these stages, the Prandtl-Reuss plasticity model, incorporating the von Mises yield criterion and an associated flow rule, is utilized to describe the material behavior. Eq. (2) describes the set of ratios for reduction factors to be applied to the CFS mechanical properties after exposure to high temperatures. Other relevant contributions include expressions for these critical mechanical properties: (i) yield strength – k_y, (ii) ultimate strength – k_u, and (iii) elastic modulus – k_E, proposed by Gunalan and Mahendran (2014 a,b), Lu *et al.* (2016), Kesawan and Mahendran (2017), Li and Young (2018), Singh and Singh (2018), Yu *et al.* (2019), Cai and Young (2019), Chen *et al.* (2019), Ren *et al.* (2020), Pandey and Young (2021), and Shi *et al.* (2022) – refer to Tables 1, 2, and 3 for detailed values.

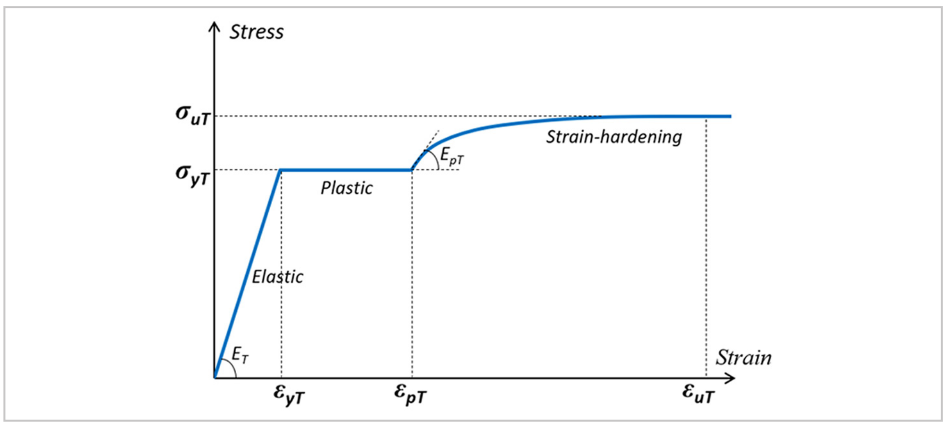

Figure 3 - Typical Stress-Strain model.

$$\sigma = \begin{cases} E_T\varepsilon & 0 \le \varepsilon < \varepsilon_{yT} \\ \sigma_{yT} & \varepsilon_{yT} \le \varepsilon < \varepsilon_{pT} \\ \sigma_{uT} - (\sigma_{uT} - \sigma_{yT})\left(\dfrac{\varepsilon_{uT} - \varepsilon}{\varepsilon_{uT} - \varepsilon_{pT}}\right)^{\rho} & \varepsilon_{pT} \le \varepsilon < \varepsilon_{uT} \\ \sigma_{uT} & \varepsilon_{uT} \le \varepsilon \end{cases} \qquad (1)$$

where, $\rho = E_{pT}\left(\dfrac{\varepsilon_{uT} - \varepsilon_{pT}}{\sigma_{uT} - \sigma_{yT}}\right)$

E_T is the residual elastic modulus; σ_{yT} and σ_{uT} are the residual yield and ultimate strengths, respectively; ε_{yT} is the yield strain (σ_{yT} / E_T).

$$k = \begin{cases} k_y = \sigma_{yT} / \sigma_y \\ k_u = \sigma_{uT} / \sigma_u \\ k_E = E_T / E \end{cases} \qquad (2)$$

Table 1 - Parameters and analytical expressions for k_y proposed by researchers for CFS.

Author	σ_y (MPa)	k_y	
GM	< 500	$1.005 - 0.00024\,T$ $2.02 - 0.0018\,T$	$20\,°C \le T \le 650\,°C$ $650\,°C \le T \le 800\,°C$
	≥ 500	1.0 $-3.5 \times 10^{-6}\,T^2 + 2.15 \times 10^{-3}\,T + 0.67$ $3.8 \times 10^{-5}\,T^2 - 4.63 \times 10^{-2}\,T + 14.52$ $0.63 - 0.00035\,T$	$20\,°C \le T \le 300\,°C$ $300\,°C < T \le 500\,°C$ $500\,°C < T \le 600\,°C$ $600\,°C < T \le 800\,°C$
Lu	235	$1.004 - 5.76 \times 10^{-5}\,T - 3.72 \times 10^{-7}\,T^2$	$20\,°C \le T \le 800\,°C$
KM	350 and 450	1 $-0.0008\,T + 1.22$	$20\,°C \le T \le 300\,°C$ $300\,°C < T \le 800\,°C$
LY	700 and 900	$1 - \frac{T - 20}{30000}$ $0.984 - \frac{(T - 500)^{2.5}}{1600000}$ $0.366 - \frac{T - 750}{100000}$	$20\,°C < T \le 500\,°C$ $500\,°C < T \le 750\,°C$ $750\,°C < T \le 1000\,°C$
SS		1 $-0.0000003 \times T^2 - 0.0006 \times T + 1.2033$	$20\,°C \le T \le 300\,°C$ $300\,°C < T \le 802\,°C$
Yu	< 500	1 $1 - 8.55 \times 10^{-4}\,(T - 300)$	$20\,°C < T \le 300\,°C$ $300\,°C < T \le 1000\,°C$
	≥ 500	1 $1 - \frac{0.629\,(T - 400)}{200}$ 0.371	$20\,°C < T \le 400\,°C$ $400\,°C < T \le 600\,°C$ $600\,°C < T \le 1000\,°C$
CY	450, 500 and 550	$1 - \frac{(T - 20)^1}{3.500 \times 10^3}$ $0.92 - \frac{(T - 300)^6}{5.813 \times 10^{14}}$ $0.50 - \frac{(T - 550)^{0.3}}{3.220 \times 10^1}$	$20\,°C < T \le 300\,°C$ $300\,°C < T \le 550\,°C$ $550\,°C < T \le 900\,°C$
Ch	345	1.0 $-3.300 \times 10^{-3} - 3.203 \times 10^{-6}\,T + 0.156$ $-4.482 \times 10^{-4}\,T + 1.204$ $-3.840 \times 10^{-3}\,T + 4.256$	$20\,°C < T \le 500\,°C$ $500\,°C < T \le 700\,°C$ $700\,°C < T \le 900\,°C$ $900\,°C < T \le 1000\,°C$
	550	1.0 $4.480 \times 10^{-3} - 5.220 \times 10^{-6}\,T + 0.038$ $6.482 \times 10^{-2} - 6.374 \times 10^{-5}\,T - 15.508$ $-3.327 \times 10^{-4}\,T + 0.628$	$20\,°C < T \le 400\,°C$ $400\,°C < T \le 500\,°C$ $500\,°C < T \le 600\,°C$ $600\,°C < T \le 800\,°C$
Re	235	0.97 $0.78 + 9.50 \times 10^{-4}\,T$ 1.35	$20\,°C \le T \le 200\,°C$ $200\,°C < T \le 600\,°C$ $600\,°C < T \le 800\,°C$
PY	690 to 1070	$1 - \frac{(T - 28)}{5000}$ $0.9456 - \frac{(T - 300)^{2.8}}{3 \times 10^7}$ 0.3020	$28\,°C < T \le 300\,°C$ $300\,°C < T \le 700\,°C$ $700\,°C < T \le 1200\,°C$
Sh	345	1 $0.8441\left(\frac{T}{500} - 1\right)^4 - 0.5259\left(\frac{T}{500} - 1\right)^3 - 0.4818\left(\frac{T}{500} - 1\right)^2 + 1$	$20\,°C < T \le 500\,°C$ $500\,°C < T \le 1000\,°C$

Table 2 - Parameters and analytical expressions for k_u proposed by researchers for CFS.

Author	σ_y (MPa)	k_u	
GM	< 500	$1.002 - 0.000104\,T$ $1.114 - 0.00033\,T$	20 °C ≤ T ≤ 500 °C 500 °C ≤ T ≤ 800 °C
	≥ 500	1.0 $-2.5\times10^{-6}\,T^2 + 1.45\times10^{-3}\,T + 0.79$ $3.8\times10^{-5}\,T^2 - 4.57\times10^{-2}\,T + 14.24$ $0.56 - 0.0001\,T$	20 °C ≤ T ≤ 300 °C 300 °C < T ≤ 500 °C 500 °C < T ≤ 600 °C 600 °C < T ≤ 800 °C
Lu	235	$0.992 + 3.97\times10^{-4}\,T - 1.76\times10^{-6}\,T^2 + 1.37\times10^{-9}\,T^3$	20 °C ≤ T ≤ 1000 °C
KM	350 and 450	1 $-0.0006\,T + 1.18$	20 °C ≤ T ≤ 300 °C 300 °C < T ≤ 800 °C
LY	700 and 900	$1 - \frac{(T-20)^{2.5}}{29000000}$ $0.504 - \frac{(T-750)}{12000}$	20 °C < T ≤ 750 °C 750 °C < T ≤ 1000 °C
SS		1 $-0.0006\times T + 1.1753$	20 °C ≤ T ≤ 300 °C 300 °C < T ≤ 802 °C
Yu	< 500	1 $1 - 6.283\times10^{-4}\,(T-300)$	20 °C < T ≤ 300 °C 300 °C < T ≤ 1000 °C
	≥ 500	1 $1 - \frac{0.518\,(T-400)}{200}$ 0.482	20 °C < T ≤ 400 °C 400 °C < T ≤ 600 °C 600 °C < T ≤ 1000 °C
CY	450, 500 and 550	$1 - \frac{(T-20)^1}{2.800\times10^3}$ $0.90 - \frac{(T-300)^6}{6.425\times10^{14}}$ $0.52 - \frac{(T-550)^{0.3}}{8.280\times10^1}$	20 °C < T ≤ 300 °C 300 °C < T ≤ 550 °C 550 °C < T ≤ 900 °C
Ch	345	$-4.186\times10^{-6}\,T^2 - 1.163\times10^{-7}\,T + 1.00$ $4.980\times10^{-3} - 4.782\times10^{-6}\,T - 0.334$ $6.070\times10^{-3}\,T^2 - 3.704\times10^{-6}\,T - 1.631$ $-0.003\times T + 3.285$	20 °C < T ≤ 500 °C 500 °C < T ≤ 700 °C 700 °C < T ≤ 900 °C 900 °C < T ≤ 1000 °C
	550	$9.577\times10^{-5}\,T^2 - 4.420\times10^{-7}\,T + 0.999$ $4.697\times10^{-2}\,T^2 - 4.643\times10^{-5}\,T - 10.943$ $-2.383\times10^{-4}\,T^2 + 0.658$	20 °C < T ≤ 500 °C 500 °C < T ≤ 600 °C 600 °C < T ≤ 800 °C
Re	235	1	20 °C ≤ T ≤ 800 °C
PY	690 to 1070	1 $1 - \frac{(T-300)^{2.45}}{3.6\times10^6}$ 0.3412	28 °C < T ≤ 300 °C 300 °C < T ≤ 700 °C 700 °C < T ≤ 1200 °C
Sh	345	1 $-0.3431\left(\frac{T}{500}-1\right)^4 - 1.187\left(\frac{T}{500}-1\right)^3 - 0.91\left(\frac{T}{500}-1\right)^2 + 1$	20 °C < T ≤ 500 °C 500 °C < T ≤ 1000 °C

Table 3 - Parameters and analytical expressions for k_E proposed by researchers for CFS.

Author	σ_y (MPa)	k_E	
GM	< 500	1 1.28 - 0.0004 T	20 °C ≤ T ≤ 700 °C 700 °C ≤ T ≤ 800 °C
	≥ 500	1.0 1.15 - 0.000375 T	20 °C ≤ T ≤ 400 °C 400 °C < T ≤ 800 °C
Lu	235	$1.001 - 5.02 \times 10^{-5}\,T + 4.90 \times 10^{-8}\,T^2$	20 °C ≤ T ≤ 800 °C
KM	350 and 450	1 $- 63 \times 10^{-5}\,T + 1.317$	20 °C ≤ T ≤ 500 °C 500 °C < T ≤ 800 °C
LY	700 and 900	1 $2 \times 10^{-9}\,T^3 - 6 \times 10^{-6}\,T^2 + 0.0019\,T + 0.916$	20 °C < T ≤ 300 °C 500 °C < T ≤ 750 °C
SS		$- 0.00053 \times T + 1.0121$ 0.85	20 °C ≤ T ≤ 300 °C 300 °C < T ≤ 802 °C
CY	450, 500 and 550	$1 - \frac{(T - 20)^5}{5.227 \times 10^{14}}$ $0.92 - \frac{(T - 550)^3}{8.889 \times 10^7}$ 0.83	20 °C < T ≤ 550 °C 550 °C < T ≤ 750 °C 750 °C < T ≤ 900 °C
Ch	345	1.0 $6.080 \times 10^{-3}\,T^2 - 3.968 \times 10^{-6}\,T - 1.339$	20 °C < T ≤ 800 °C 800 °C < T ≤1000 °C
	550	1.0	20 °C < T ≤ 800 °C
PY	690 to 1070	$1 - \frac{(T - 28)}{8000}$ $0.9223 - \frac{(T - 650)^{1.5}}{55000}$	28 °C < T ≤ 650 °C 650 °C < T ≤ 1200 °C
Sh	345	1	20 °C < T ≤ 1000 °C

4. Results and Discussion

This section presents a parametric numerical study conducted to evaluate the influence of post-fire conditions – namely, elevated temperatures followed by air cooling – on the constitutive behavior of a CFS C200 column. The study encompassed a total of *770* cases, derived from the combination of *7* temperatures, *10* yield stresses, and *11* different sets of expressions for the reduction factors proposed in the literature (already listed in Tables 1, 2, and 3).

The reduction factors obtained from these studies were integrated into the numerical model implemented in ANSYS (SAS, 2009). This analysis provides a comprehensive assessment of the impact of post-fire conditions on the mechanical properties of CFS, with the results thoroughly examined in the subsequent sections.

4.1 Post-buckling response of CFS LC columns

This section examines the distortional elastic-plastic post-buckling behavior of lipped channel columns, with particular emphasis on the influence of elevated temperatures resulting from post-fire conditions. As detailed in Section 3.1, the post-fire CFS constitutive model used in this analysis is based on the analytical formulations proposed by Gunalan and Mahendran (2014 a,b).

Figure 4(a) depicts the nonlinear equilibrium paths (P / $P_{cr.D.20}$ versus $|\delta|/t$) for columns concerning $\lambda_{D.20}$ = 1.875 and exposed to post-fire temperatures (*T=20–300–400–500–600–700–800* °C). The white markers identify the normalized failure loads ($P_{u.T}$) relative to the critical buckling loads at room temperature ($P_{cr.D.20}$). The plots also include elastic response curves for moderate temperatures, provided for comparative analysis, along with elastic-plastic response curves for elevated temperatures. At this stage of the research, special emphasis is placed on analyzing the deformed configurations and von Mises stress distributions, as shown in Figure 4(b). These responses were captured precisely at the collapse stage, when $P = P_{u.T}$, for columns subjected to temperatures of *300–600–800* °C, serving as examples and providing critical insights into the observed phenomena. Following a thorough analysis of the results, the subsequent observations can be drawn:

(i) As anticipated, the equilibrium paths of the columns display a gradual downward shift as the temperature increases, reflecting a concomitant reduction in the failure loads.

(ii) Considering that the effects of thermal actions are negligible – due to the uniform temperature distribution and the lack of restraint against deformation, the distortional failure modes remain largely independent of the temperature. As a result, these modes display highly similar configurations across all analyzed columns, as depicted in Fig. 4(b).

(iii) The above remark also applies to the associated von Mises stress distributions, which exhibit both qualitative and, to a reasonable extent, quantitative similarities across the various temperature conditions, akin to those observed at room temperature. Naturally, the stress magnitudes progressively decrease as the temperature rises, reflecting the continuous degradation of the material properties of the steel.

(iv) Furthermore, the spread of plasticity in the flange, related to the formation of the 'distortional plastic hinge', progressively reduces with increasing temperature. This behavior is attributed to the temperature-dependent nature of the stress-strain relationship, where the yield stress reduction factors are more significant at lower temperatures and diminish as the temperature increases.

(v) Finally, note that all $P_{u.T}$ / $P_{cr.D.20}$ lie above the point where this ratio equals one. This indicates a slight increase in residual strength when the columns, after being subjected to post-fire elevated temperatures, are analyzed at room temperature.

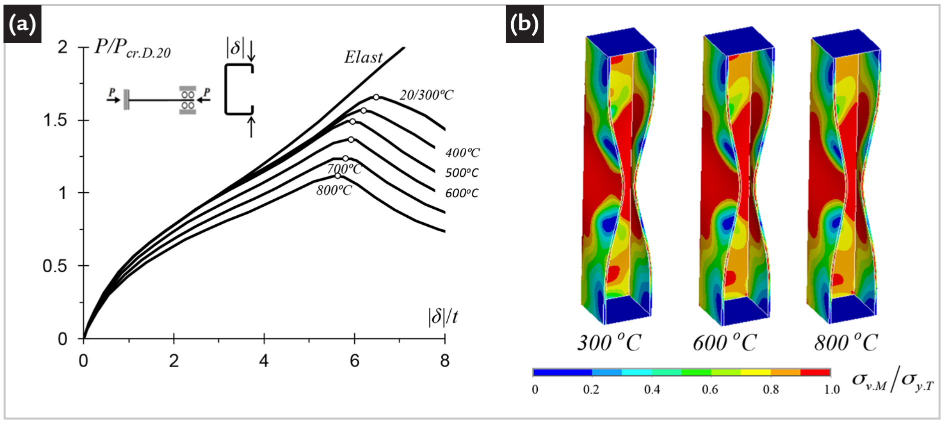

Figure 4 - Nonlinear distortional response of CFS LC columns: (a) equilibrium paths for $\lambda_{D.20}$ = 1.875 (*T=20–300–400–500–600–700–800* °C) and (b) deformed configuration and von Mises stress distributions at collapse, for $\lambda_{D.20}$ = 1.875 (*T= 300–600–800* °C).

4.2 Distortional failure load data

This section presents the results of a parametric study conducted to generate failure load data, which will form the foundation for developing and assessing the effectiveness of DSM design approaches specifically aimed at addressing column distortional failures under post-fire conditions. According to the currently codified DSM distortional design curve (considering room temperature) (AISI, 2020), the nominal ultimate load of CFS columns governed by distortional modes is determined by the following equation:

$$P_{n.D.20} = \begin{cases} P_{y.20} & \lambda_{D.20} \leq 0.561 \\ P_{y.20}\left[1 - 0.25\left(\dfrac{P_{cr.D.20}}{P_{y.20}}\right)^{0.6}\right]\left(\dfrac{P_{cr.D.20}}{P_{y.20}}\right)^{0.6} & \lambda_{D.20} \geq 0.561 \end{cases} \tag{3}$$

where (i) $P_{cr.D.20}$ and $P_{y.20}$ are the column distortional critical buckling and yield loads, respectively, and (ii) $\lambda_{D.20} = (P_{y.20} / P_{cr.D.20})^{0.5}$ is the column distortional slenderness.

A total of *770* columns are analyzed, corresponding to the following combination: (i) a single geometry, as illustrated in Figure 1; (ii) fixed (F) end support condition; (iii) *7* uniform temperatures (*T=20–300–400–500–600–700–800* °C), (iv) *10* room temperature yield stresses, covering a broad range of distortional slenderness values ($\lambda_{D.T}$ varies from *0.20* to *3.61*) and (v) *11* different sets of equations (refer to Tables 1, 2, and 3) for the mechanical property reduction factors. Figure 5 plots the failure load ratios $P_{u.T}$ / $P_{y.T}$ against $\lambda_{D.T}$ for each temperature value, alongside the corresponding DSM strength curve for comparison. The analysis of these plots leads to the following conclusions:

(i) The $P_{u.T}$ / $P_{y.T}$ versus $\lambda_{D.T}$ data, regardless of temperature, closely align with the typical pattern of 'Winter-type' strength curves, exhibiting little variation across the full range of slenderness considered.

(ii) Based on the findings discussed in the above sections of this work, it is evident that the existing DSM strength curves effectively predict the post-fire distortional failure loads of columns with slenderness ratios ranging from low to high (*0.20* ≤ λ ≤ *3.61*). Consequently, there is no need to modify or reduce the current DSM design curve to improve the accuracy of failure load predictions.

(iii) However, due to the limitations of the current study, further data is required to enhance the robustness of the findings. This includes exploring a wider range of cross-sectional dimensions and shapes, evaluating different support conditions, and considering various cooling parameters. Additionally, factors such as loading conditions, material variability, and potential interactions between fire exposure and long-term service conditions should be incorporated into future analyses. Only with a more comprehensive dataset, encompassing a broader spectrum of variables and scenarios, can a more generalized and reliable conclusion be drawn regarding the post-fire distortional failure behavior of cold-formed steel columns.

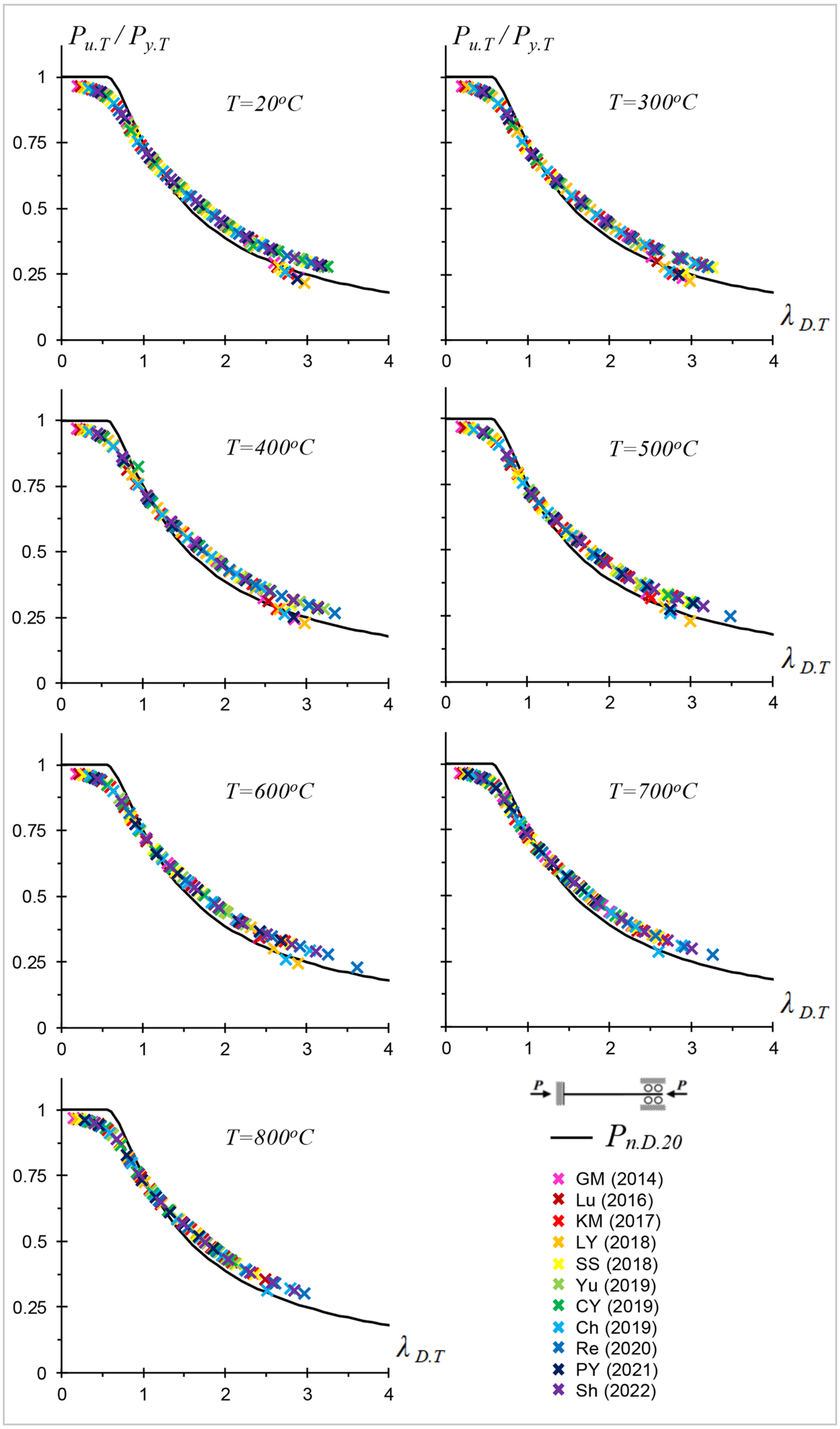

Figure 5 - P_u / P_y vs. $\lambda_{D.T}$ for temperatures (*T=20–300–400–500–600–700–800* ºC) data obtained in this study, compared with the DSM codified strength curve.

5. Concluding remarks

This article reported the most recent numerical (ANSYS SFEA) results of an ongoing investigation on the post-buckling behavior, ultimate strength and DSM design of CFS columns failing in distortional modes under post-fire conditions. These results cover a total of *770* columns characterized by: (i) a lipped channel cross-sectional geometry with a length selected to ensure pure distortional buckling and failure modes, (ii) fixed-end support conditions, (iii) sets of temperature-dependent post-fire steel properties from various sources (Gunalan and Mahendran, 2014 a,b; Lu *et al.*, 2016; Kesawan and Mahendran, 2017; Li and Young, 2018; Singh and Singh, 2018; Yu *et al.*, 2019; Cai and Young, 2019; Chen *et al.*, 2019; Ren *et al.*, 2020; Pandey and Young, 2021; Shi *et al.*, 2022) for flat specimens after air cooling, (iv) *10* room-temperature yield stresses, allowing coverage of wide range of distortional slenderness ($\lambda_{D.T}$ varying from *0.20* to *3.61*) and (v) *7* uniform temperatures (*T=20–300–400–500–600–700–800* °C).

Following the validation of the numerical model against ultimate load results from Gunalan and Mahendran (2014 a,b), a comprehensive parametric study was conducted to compile an extensive dataset of post-fire distortional failure loads for CFS columns.

A series of elastic-plastic distortional post-buckling results were presented and analyzed to better understand the combined effects of (i) temperature levels on the distortional structural behavior and (ii) the load-bearing capacity of CFS columns subjected to post-fire conditions. One key objective was to extend the findings of Gunalan and Mahendran (2014 a,b) — originally focused on short-lipped channel columns made from varying steel grades (*G300, G500* and *G550*) and thicknesses (*0.95, 1.00* and *1.15* mm) – to include a wider range of CFS columns in post-fire conditions. Additionally, the study aimed to assess whether the current DSM design rules can accurately predict the ultimate strengths of compression members failing in distortional buckling after exposure to elevated temperatures. Among the key findings of this study, the following are particularly noteworthy:

(i) Regardless of the temperature, the $P_{u.T}$ / $P_{y.T}$ versus $\lambda_{D.T}$ data clusters closely adhere to the characteristic pattern of "Winter-type" strength curves, with minimal dispersion observed across the entire range of slenderness values.

(ii) The analysis demonstrated that the failure load predictions based on the DSM design approach are generally accurate and tend to be conservative for columns with slenderness values ranging from low to high ($0.20 \leq \lambda \leq 3.61$).

(iii) Although the analyzed columns were subjected to post-fire conditions, an increase in residual strength was observed, indicating slightly higher ultimate strengths for these compression members failing in distortional buckling. It is important to note that while these structures underwent post-fire events, both the distortional buckling analyses and DSM-based predictions were conducted under room temperature conditions.

(iv) Due to the limitations of the current study, further data is needed, including additional cross-sectional dimensions, support conditions, and cooling parameters (natural air cooling, forced air, or water quenching). Future research should also consider factors such as loading conditions, material variability, fire duration, service conditions and studies involving transient state (non-uniform temperature distributions). A more comprehensive dataset will enable a broader and more reliable conclusion regarding the post-fire behavior of cold-formed steel columns.

(v) The study's findings suggest that engineers can use standard DSM provisions to estimate the post-fire capacity of cold-formed steel columns, provided the mechanical properties are adjusted to reflect degradation due to elevated temperatures. The results demonstrate that, even after fire exposure followed by natural cooling, residual distortional strength remains conservatively predictable using the current DSM equations. Practically, this implies that engineers could assess the reuse potential of cold-formed steel columns after fire events using post-fire reduction factors (as compiled in this study) and the standard DSM framework.

Acknowledgements

The first and third authors gratefully acknowledge the financial support of the Brazilian institutions (i) CAPES (Coordenação de Aperfeiçoamento de Pessoal de Nível Superior) – Finance Code 001 (1st and 3rd authors), (ii) CNPq (Conselho Nacional de Desenvolvimento Científico e Tecnológico) – Finance Codes 140103/2019-8 (first author) and 313197/2020-2 (third author) and (iii) FAPERJ (Fundação Carlos Chagas Filho de Amparo à Pesquisa do Estado do Rio de Janeiro) – Finance Code E-26/200.959/2021 (third author).

References

ABAQUS version 6.7. ***User manual***, 2007. Hibbitt. Karlsson & Sorenson. Inc.

ASSOCIAÇÃO BRASILEIRA DE NORMAS TÉCNICAS. ***ABNT NBR 14762:2010***: dimensionamento de estruturas de aço constituídas por perfis formados a frio. Rio de Janeiro, 2010.

BEBIANO, R.; PINA, P.; SILVESTRE, N.; CAMOTIM, D. GBTUL ***1.0***β ***- code for buckling and vibration analysis of Thin-Walled Members***, DECivil/IST, Technical University of Lisbon, 2008a. Disponível em: http://www.civil.ist.utl.pt/gbt.

BEBIANO, R.; SILVESTRE, N.; CAMOTIM, D. GBTUL – a code for the buckling analysis of cold formed steel members. ***In***: INTERNATIONAL SPECIALTY CONFERENCE ON RECENT RESEARCH AND DEVELOPMENTS IN COLD-FORMED STEEL DESIGN AND CONSTRUCTION, 19, St. Louis, 14-15 out. ***Proceedings*** [...]. R LaBoube, WW Yu (ed.), p.61-79, 2008b.

BOERAEVE, P. H.; LOGNARD, B.; JANSS, J.; GERARDY, J. C.; SCHLEICH, J. B. Elasto-plastic behaviour of steel frame works. ***Journal of Constructional Steel Research,*** v. 27, p. 3-21, 1993.

B.S.I. ***Structural use of steelwork in building***: code of practice for fire resistant design. British Standard Institution. 1990. part 8.

CAI, Y.; YOUNG, B. Mechanical properties of thin sheet after exposure to high temperatures. ***Thin-Walled Structures,*** v. 142, p. 460-475, 2019.

CECS 252:2009. ***Standard for building structural assessment after fire.*** China Planning Press. Beijing, China, 2009.

CHEN, W.; YE, J.; PENG, J.; LIU, B. Experimental investigation of post-fire mechanical properties of Q345 and G550 cold-formed steel. ***Journal of Materials in Civil Engineering,*** 2019.

ELLOBODY, E.; YOUNG, B. Behaviour of cold-formed steel plain angle columns. ***Journal of Structural Engineering*** (ASCE), v. 131, n. 3, p. 457-466, 2005.

GUNALAN, S.; MAHENDRAN, M. Experimental investigation of post-fire mechanical properties of cold-formed steels. ***Thin-Walled Structures,*** v. 84, p. 241-254, 2014a.

GUNALAN, S.; MAHENDRAN, M. Experimental and numerical studies of fire exposed lipped channel columns subject to distortional buckling. ***Fire Safety Journal,*** v. 70, p. 34-45, 2014b.

KESAWAN, S.; MAHENDRAN, M. Post-fire mechanical properties of cold-formed steel hollow section. ***Construction and Building Materials,*** v. 161, p. 26-36, 2018.

LANDESMANN, A.; CAMOTIM, D. On the distortional buckling, post-buckling and strength of cold-formed steel lipped channel columns under fire conditions. ***Journal of Structural Fire Engineering,*** v. 2, n. 1, p. 1-19, 2011.

LI, H.-T.; YOUNG, B. Residual mechanical properties of high strength steels after exposure to fire. ***Journal of Construction Steel Research,*** v. 148, p. 562-571, 2018.

LU, J.; LIU, H.; CHEN, Z.; LIAO, X. Experimental investigation into the post-fire mechanical properties of hot-rolled and cold-formed steels. ***Journal of Constructional Steel Research,*** v. 121, p. 291-310, 2016.

MANDER, J. B. ***Seismic design of bridge piers,*** PH.D. (Thesis) - University of Canterbury, Christchurch, New Zealand, 1983.

NORTH AMERICAN SPECIFICATION - NAS. ***AISI-S100-16 w/S3-22***: for the design of cold-formed steel structural members (2016 edition reaffirmed in 2020 with Supplement 3). Washington DC, American Iron and Steel Institute.

OUTINEN, J.; MÄKELÄINEN, P. Mechanical properties of structural steel at elevated temperatures and after cooling down. ***Fire and Materials,*** v. 28, p. 237-251, 2004.

PANDEY, M.; YOUNG, B. Post-fire mechanical response of high strength steels. ***Thin-Walled Structures,*** v. 164, n. 107606, 2021.

PROLA, L. C.; CAMOTIM, D. On the distortional post-buckling behavior of cold-formed lipped channel steel columns. *In*: ANNUAL STABILITY CONFERENCE - SSRC 2002, Seattle, 24-27 abr. ***Proceedings*** [...]. p. 571-590, 2002a.

PROLA, L. C.; CAMOTIM, D. On the distortional post-buckling behaviour of rack-section cold-formed steel columns. *In*: INTERNATIONAL CONFERENCE ON COMPUTATIONAL STRUCTURES TECHNOLOGY - CST, 2002, 6, Prague, 4-6 sept. ***Proceedings*** [...]. B. Topping, Z. Bittnar (ed.), Civil-Comp Press (Stirling), p. 233-234. (full paper in CD-ROM 2002b).

REN, C.; DAI, L.; HUANG, Y.; HE, W. Experimental investigation of post-fire mechanical properties of Q235 cold-formed steel. ***Thin-Walled Structures,*** v. 150, p. 1-16, 2020.

SAS - Swanson Analysis Systems Inc. ***ANSYS Reference Manual*** (version 12), 2009.

SCHAFER, B. W. Review: the Direct Strength Method of cold-formed steel member design. ***Journal of Constructional Steel Research,*** v. 64, n. 7-8, p. 766-788, 2008.

SHI, G.; WANG, S.; RONG, C. Experimental investigation into mechanical properties of Q345 steel after fire. ***Journal of Construction Steel Research,*** v. 199, n. 107582, 2022.

SILVESTRE, N.; CAMOTIM, D. Local-plate and distortional post-buckling behavior of cold-formed steel lipped channel columns with intermediate stiffeners. ***Journal of Structural Engineering - ASCE*** 132, n. 4, p. 529-540, 2006.

SINGH, T. G.; SINGH, K. D. Post-fire mechanical properties of YSt-310 cold-formed tubular sections. ***Journal of Construction Steel Research,*** v. 153, p. 654-666, 2019.

STANDARDS OF AUSTRALIA – SA/ STANDARDS OF NEW ZEALAND – SNZ. ***AS/NZS 4600***: Cold-Formed Steel Structures (3rd edition). AS/NZS 4600:2018, Sydney-Wellington, Standards of Australia and Standards of New Zealand.

WANG, X. Q.; TAO, Z.; UY, B. Stress-strain curves of structural steel after exposure to elevated

Temperatures. *In*: INTERNATIONAL CONFERENCE ON ADVANCES IN STEEL CONCRETE COMPOSITE AND HYBRID STRUCTURES, 10, Singapore. ***Proceedings*** [...]. p. 833-40, 2012.

YU, Y.; LAN, L.; DING, F.; WANG, L. Mechanical properties of hot-rolled and cold-formed steels after exposure to elevated temperature: a review. ***Construction and Building Materials,*** v. 213, p. 360-376, 2019.

Received: 24 January 2025 - Accepted: 30 July 2025.

Authors' contributions

Gabriela Ribeiro Fernandes (Corresponding author): *investigation (equal), methodology (equal), validation (equal), writing - original draft (equal);* **Fernanda Cristina Moreira da Silva:** *investigation (equal), methodology (equal), validation (equal), writing - original draft (equal);* **Alexandre Landesmann:** *conceptualization (equal), funding acquisition (equal), supervision (equal), validation (equal), writing - review & editing (equal).*

Funding information

Conselho Nacional de Desenvolvimento Científico e Tecnológico - Proc. n° 140103/2019-8 e 313197/2020-2, Coordenação de Aperfeiçoamento de Pessoal de Nível Superior, Fundação Carlos Chagas Filho de Amparo à Pesquisa do Estado do Rio de Janeiro E-26/200.959/2021.

Conflict of interests

The authors declare that they have no conflict of interest.

Data availability

The data supporting the conclusions of this study are available in the references of this article.

Associate Editor

Naloan Coutinho Sampa